nature physics

ARTICLES

PUBLISHED ONLINE: 24 AUGUST 2015 | DOI: 10.1038/NPHYS3434

Effect of magnetic frustration on nematicity and superconductivity in iron chalcogenides

J. K. Glasbrenner[1]*, I. I. Mazin[2], Harald O. Jeschke[3], P. J. Hirschfeld[4], R. M. Fernandes[5] and Roser Valentí[3]

Over the past few years iron chalcogenides have been intensively studied as part of the wider family of iron-based superconductors, with many intriguing results reported so far on intercalated and monolayer FeSe. Nevertheless, bulk FeSe itself remains an unusual case when compared with pnictogen-based iron superconductors, and may hold clues to understanding the more exotic derivatives of the FeSe system. The FeSe phase diagram is distinct from the pnictides: the orthorhombic distortion, which is likely to be of a 'spin-nematic' nature in numerous pnictides, is not accompanied by magnetic order in FeSe, and the superconducting transition temperature T_c rises significantly with pressure before decreasing. Here we show that the magnetic interactions in FeSe, as opposed to most pnictides, demonstrate an unusual and unanticipated frustration, which suppresses magnetic (but not nematic) order, triggers ferro-orbital order in the nematic phase and can naturally explain the non-monotonic pressure dependence of the superconducting critical temperature $T_c(P)$.

Although full consensus regarding the mechanism of high-temperature superconductivity in Fe-based superconductors (FeBS) remains elusive, nearly all researchers agree that it is unconventional and that it has a magnetic origin[1,2]. However, there is a divergence of opinion on the nature of the electrons responsible for magnetism. There is an itinerant approach based on calculating the spin susceptibility with moderate Coulomb (Hubbard) and Hund's interactions[3–9] as well as a localized approach where itinerant electrons responsible for conduction and the Fermi surface interact with local spins[10,11]. Finally, there is an increasingly popular description where the electrons have a dual character and provide the local moments, the interaction between them, and the electronic conductivity[12–15]. Within this picture, FeBS can still be reasonably mapped onto a short-range model of pairwise interactions between the local moments.

Following the discovery of the FeBS, there were multiple attempts to map the magnetic interactions onto the Heisenberg model. The J_1–J_2 model on the square lattice[16] with nearest-neighbour (J_1) and next-nearest-neighbour (J_2) exchange couplings was a natural starting point that required markedly different couplings for ferro- and antiferromagnetic neighbours, $J_{1a} \ll J_{1b}$, to reproduce the observed spin waves[17,18] and *ab initio* calculations[19]; it also failed to describe the double-stripe configuration (see Fig. 1 for pattern definition) in FeTe (refs 20,21). The model was extended to include third-neighbour exchange J_3 (ref. 22) to reproduce the FeTe magnetic ground state. However, only the Ising model has this configuration as a solution, and in the Heisenberg model it is not a ground state for any set of parameters[23,24]. Therefore adding J_3 does not solve the problem. Furthermore, $J_{1a} \ll J_{1b}$ implies an unphysical temperature dependence of the exchange constants, because, as T approaches T_N, $J_{1a} \to J_{1b}$ by symmetry.

There were attempts to overcome these problems by adding the nearest-neighbour biquadratic exchange interaction $K(\mathbf{S}_i \cdot \mathbf{S}_j)^2$ to the J_1–J_2 (refs 19,25) or J_1–J_2–J_3 (ref. 26) Heisenberg model. The three-neighbour Heisenberg model with biquadratic term (denoted J_1–J_2–J_3–K model from now on) eliminates the need for the $J_{1a,1b}$ anisotropy of the nearest-neighbour exchange and, for sufficiently large K and J_3, has a ground state consistent with that of FeTe. The biquadratic coupling in this model is also essential to explain the splitting between the antiferromagnetic and orthorhombic phase transitions in the Fe pnictides[27,28].

Whereas the magnetism in Fe pnictides is qualitatively explained by the J_1–J_2–J_3–K model, the Fe chalcogenides remain problematic. Specifically, there are two important unresolved controversies regarding bulk FeSe. First, it shows a structural transition at $T_s \sim 90$ K but, contrary to the Fe pnictides, no magnetic order is observed below T_s. Instead, an extended nematic region is detected[29,30] and the system becomes superconducting at $T_c \sim 8$ K. Second, the superconducting T_c first increases with pressure and then decreases, forming a dome[31]. This is in apparent contradiction with the expectation of a decreasing T_c with pressure when magnetism is absent.

In the present work we propose a solution to this mystery and generalize the results to the family of Fe chalcogenides FeSe/Te. We show, using *ab initio* density functional theory calculations and effective model considerations, that both controversies are related to unusual magnetic frustration, absent in most pnictides. Further, we propose a phenomenological model that reflects our density functional theory findings and their relation to nematic order in FeSe.

We also show that J_1–J_2–J_3–K is the minimal spin model that includes the relevant complexity of the low-energy magnetism in Fe chalcogenides. Although a complete description of magnetic excitations in FeBS in terms of a local spin model seems impossible owing to considerable itinerancy (as manifested already by the relatively large values of J_3 and K), the local energy physics can be reasonably well visualized with the help of the J_1–J_2–J_3–K model. Here we provide, for the first time, the full mean-field phase diagram for this model, which illustrates our *ab initio* findings.

[1]National Research Council/Code 6393, Naval Research Laboratory, Washington DC 20375, USA. [2]Code 6393, Naval Research Laboratory, Washington DC 20375, USA. [3]Institut für Theoretische Physik, Goethe-Universität Frankfurt, 60438 Frankfurt am Main, Germany. [4]Department of Physics, University of Florida, Gainesville, Florida 32611, USA. [5]School of Physics and Astronomy, University of Minnesota, Minneapolis, Minnesota 55455, USA. e-mail: james.glasbrenner.ctr@nrl.navy.mil

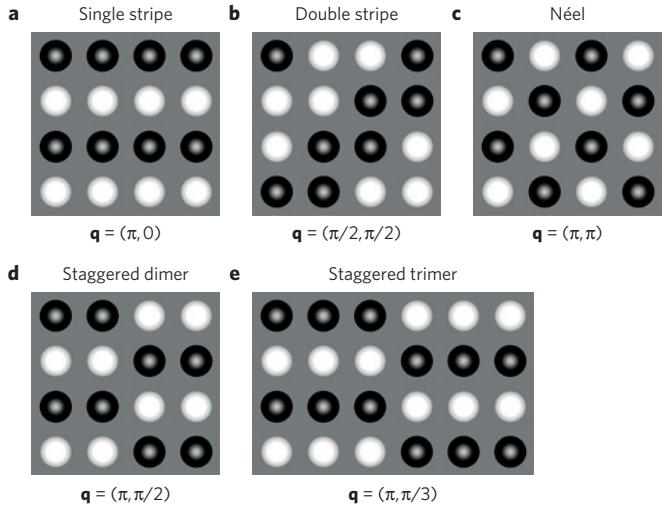

Figure 1 | Collinear magnetic structures used for fitting the J_1–J_2–J_3–K model. Single stripe (**a**), double stripe (**b**) chequerboard (Néel) (**c**), staggered dimer (**d**) and staggered trimer (**e**) state.

Exchange model and phase diagram

We define the J_1–J_2–J_3–K model on the square lattice as

$$H = \sum_{\mathrm{nn}} [J_1 \hat{\mathbf{m}}_i \cdot \hat{\mathbf{m}}_j - K(\hat{\mathbf{m}}_i \cdot \hat{\mathbf{m}}_j)^2] + \sum_{\mathrm{2nn}} J_2 \hat{\mathbf{m}}_i \cdot \hat{\mathbf{m}}_j + \sum_{\mathrm{3nn}} J_3 \hat{\mathbf{m}}_i \cdot \hat{\mathbf{m}}_j \quad (1)$$

The first sum is taken over all nearest neighbour $\{i, j\}$ pairs of Fe spins, the second sum over all next nearest neighbours, and so on. $\hat{\mathbf{m}}$ is the unit vector in the spin direction, $|\hat{\mathbf{m}}_i| \equiv 1$. For $K = 0(\infty)$, this model reduces to the already solved Heisenberg[24] (Ising[32]) models on the square lattice.

To begin, we review the phase diagrams for the standard J_1–J_2–J_3 Ising and Heisenberg models. In Fig. 2a we show the mean-field $T = 0$ Ising phase diagram, which includes the staggered-dimer and double-stripe ground states. Although this phase diagram can explain the *ab initio* magnetic states of FeSe and FeTe, note that the Ising model is inapplicable to low-anisotropy materials such as the pnictides and chalcogenides, and the Heisenberg model is more appropriate[19,25,26]. The mean-field phase diagram for the Heisenberg model at $T = 0$ is shown in Fig. 2b (quantum corrections introduce minor changes[24]). The double-stripe phase has measure zero [it is a degenerate case of $\mathbf{q} = (Q, Q)$]. This means that no Heisenberg model can explain the formation of a collinear double-stripe state.

The review of the Ising and Heisenberg phase diagrams elucidates the two theoretical problems that have been underemphasized in previous analyses of the magnetic interactions of the Fe-based superconductors, especially in the chalcogenides: first, the Heisenberg model does not account for all relevant magnetically ordered states and, by implication, does not properly describe spin fluctuations; and second, the single- and double-stripe magnetic states are not the only important ground state candidates for the chalcogenides—there is a third one, the staggered dimers, which is highly competitive, but has been routinely ignored. To address these problems the biquadratic term, K, needs to be quantitatively taken into account.

We solved the full J_1–J_2–J_3–K model (equation (1)) for general K in the mean-field limit and found six possible ground states (see Supplementary Information and Discussion). Hu *et al.*[26] attempted previously to solve this model, but missed the staggered-dimer phase[33] which, we argue, is the key to understanding FeSe. A representative example phase diagram with $K/J_1 = 0.1$ is shown in Fig. 2c. For a small, but non-zero K and J_3 the staggered-dimer phase becomes stable in a narrow ($|J_2 - J_1/2| < 2\sqrt{2KJ_3}$) interval near the critical value $J_1 = 2J_2$, and at sufficiently large J_3 ($J_3 > J_1^2/8K$) the collinear double-stripe structure is stabilized. As K grows, these collinear regions also grow, and at $K > J_1/2$ the phase diagram becomes identical to the Ising phase diagram in Fig. 2a. The complexity of the derived phase diagram calls for a full first-principles analysis of the relevant magnetic phases in FeBS, which we provide below.

First-principles calculations

We performed density functional theory (DFT) calculations to obtain parameters for equation (1) and place FeSe and FeTe into the context of the J_1–J_2–J_3–K phase diagram. There is a caveat though: owing to the itinerant character of magnetism in FeBS, mapping onto local moment models such as equation (1) has limited accuracy. A fundamental assumption of the standard Heisenberg model is that the magnetic moments are rigid, and this is an excellent assumption for systems with highly localized electrons, such as the high-T_c cuprates, but relatively poor for itinerant electrons. Magnetic interactions in metals tend to have long-range tails, non-pairwise interactions, and the moments may depend on the magnetic ordering pattern. A clear example of the failure of the Heisenberg-biquadratic models is that the double stripe (Fig. 1b) and plaquette (see Supplementary Fig. 1p) configurations are degenerate in any such model, but in DFT the double stripe is 8 meV/Fe lower in energy than the plaquette configuration[34] for FeTe. Besides, we find that although we can describe most low-energy states in Fe(Se,Te) with reasonable accuracy, it is impossible to fit all energies presented in Figs 3 and 4 (and also Supplementary Fig. 2) even qualitatively, preserving the right hierarchy of states.

Despite these limitations, the J_1–J_2–J_3–K model is the simplest framework that accounts for all the magnetic ground states that DFT and experiment find in different FeBS, and arguably is also the most complex one that still allows an analytic solution. As we are interested in spin fluctuation-driven effects such as superconductivity and spin-nematicity, which are low-energy phenomena, we establish a set of criteria for our fits, with the main goal to select a consistent set of magnetic states and obtain parameters that reproduce the low-energy hierarchy obtained within DFT. The criteria are detailed in the Methods, and the chosen magnetic structures are shown in Fig. 1a–e.

We performed calculations for FeSe at three representative pressures of 0, 4 and 9 GPa, and for FeTe at ambient pressure (see Methods for details). In all cases we used experimental lattice and internal parameters in tetragonal structures, as discussed in Methods. We fitted to the five magnetic configurations reported in Fig. 3 and extracted the J_1, J_2 and J_3 parameters. The biquadratic term was extracted from noncollinear calculations as in ref. 34. The resulting J_1–J_2–J_3–K model parameters are reported in Table 1. Note that the standard errors reported in Table 1 reflect the fit inaccuracy, and not the much smaller errors of the underlying DFT calculations.

First of all, we confirmed that the staggered-dimer configuration[32,35] is 13 meV/Fe lower in energy than the single-stripe configuration and is the true DFT ground state for FeSe (ref. 33; see Fig. 3). The same phase is also the lowest in energy in FeTe, as long as one does not take into account the magnetoelastic coupling. The calculated energy difference between the double-stripe and staggered-dimer configurations in tetragonal FeTe is tiny, ~1–2 meV/Fe. However, on full structural relaxation into a monoclinic structure the double-stripe pattern gains more magnetoelastic energy than the staggered-dimer state (which relaxes into an orthorhombic structure) and ends up lower by a few meV, with the crystallographic distortion in agreement with experiment[20,21].

Another important result is that although the main contenders for the ground state of FeTe are the double-stripe ($\mathbf{q}_{\mathrm{ds}} = (\pi/2, \pi/2)$) and the staggered-dimer ($\mathbf{q}_{\mathrm{di}} = (\pi, \pi/2)$) structures, with the

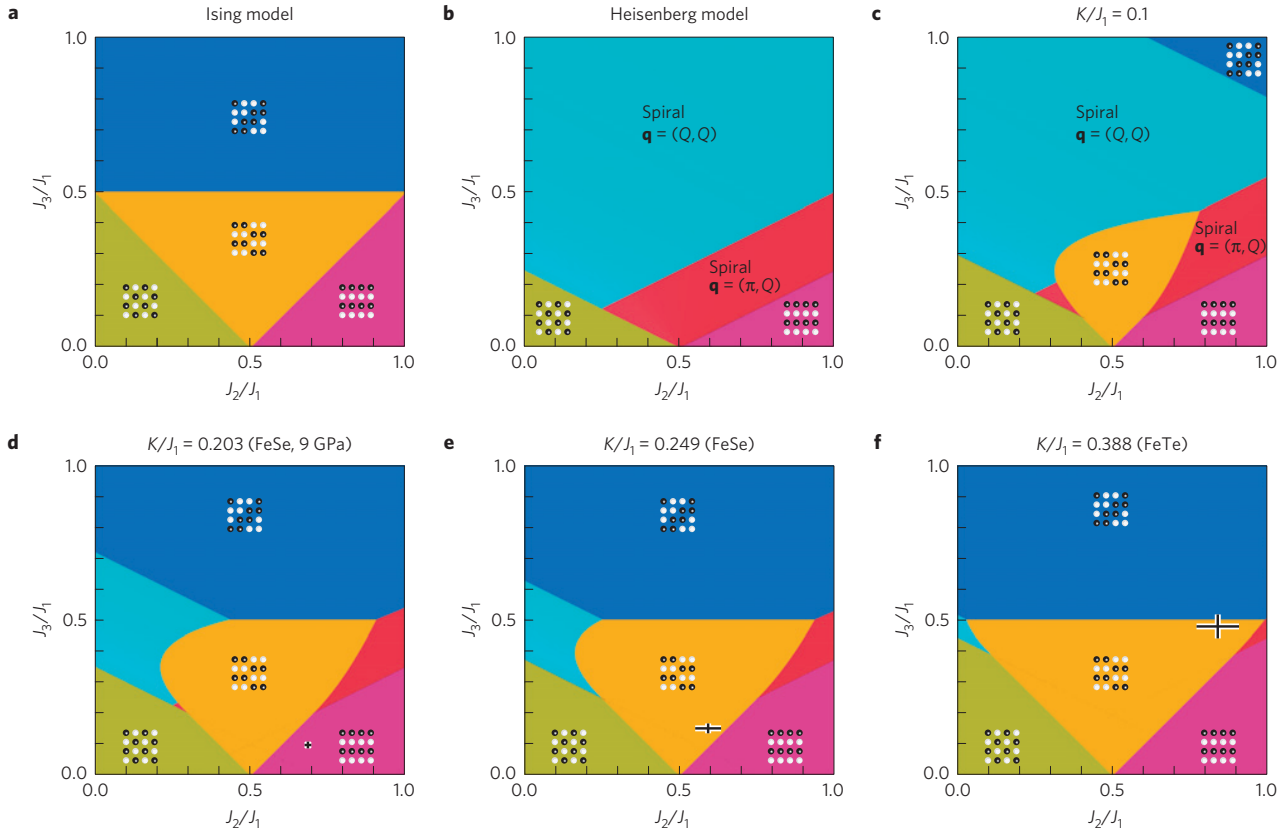

Figure 2 | Classical mean-field phase diagrams. a, The J_1–J_2–J_3 Ising model. **b**, The J_1–J_2–J_3 Heisenberg model. **c**, The J_1–J_2–J_3–K model with $K/J_1 = 0.1$. **d**, The J_1–J_2–J_3–K model with $K/J_1 = 0.20$, where the cross corresponds to FeSe at 9 GPa of pressure. **e**, The J_1–J_2–J_3–K model with $K/J_1 = 0.25$, where the cross corresponds to FeSe at 0 GPa of pressure. **f**, The J_1–J_2–J_3–K model with $K/J_1 = 0.39$, where the cross corresponds to FeTe at 0 GPa of pressure. The lengths of the cross' bars in **d**–**f** indicate the uncertainty of the fit to the J_1–J_2–J_3–K model.

staggered trimers ($\mathbf{q}_{\rm tri} = (\pi, \pi/3)$) a close third, in FeSe the double-stripe structure is not competitive at all. In FeSe the lowest energy states are the staggered dimers, trimers, tetramers and single stripes, with the respective ordering vectors $\mathbf{q}_{\rm di} = (\pi, \pi/2)$, $\mathbf{q}_{\rm tri} = (\pi, \pi/3)$, $\mathbf{q}_{\rm tetra} = (\pi, \pi/4)$ and $\mathbf{q}_{\rm ss} = (\pi, 0)$. From this, one can conclude that although in experiment the long-range order of FeSe is destroyed by spin fluctuations, the most relevant ones are those with the corresponding wavevectors listed above, and, by extension, with any $\mathbf{q} = (\pi, Q)$ such that $0 \leq Q \leq \pi/2$.

Importantly, when FeSe is structurally optimized in any of the low-energy magnetic structures, it admits an orthorhombic structure quantitatively consistent with the experiment, $(a-b)/(a+b) \sim 0.2\%$, whereas optimization without magnetism never breaks the tetragonal symmetry. Furthermore, on applying pressure, the hierarchy of states changes and the single-stripe state becomes the lowest in energy, as can be seen in Fig. 3, thus making fluctuations at $\mathbf{q}_{\rm ss} = (\pi, 0)$ the leading mode.

Discussion

As mentioned, there are two outstanding experimental paradoxes regarding FeSe. The first paradox concerns the splitting of the orthorhombic and magnetic transition observed in Fe pnictides, which is taken to an extreme in FeSe: the structural transition occurs at $T_{\rm s} \sim 90$ K, but no magnetic order follows. Yet, exactly as in the pnictides, DFT calculations reproduce the distorted structure when the calculated ground state magnetic structure is used, but show no tendency towards orbital ordering or a structural distortion if magnetization is kept zero.

The second paradox deals with the behaviour of the critical superconducting temperature with pressure $T_{\rm c}(P)$. Typically, pressure has a tendency to suppress magnetism, so—in the context of a magnetic pairing mechanism—pressure is beneficial to superconductivity when magnetic order is present, but it is destructive if it is not. For the nonmagnetic FeSe, the expectation then is that $T_{\rm c}$ should decrease monotonically with pressure. Instead, $T_{\rm c}$ first increases and then decreases with pressure, forming a characteristic dome shape[31]. In the following we discuss how the J_1–J_2–J_3–K model resolves these paradoxes.

Table 1 | Heisenberg and biquadratic exchange parameters for FeSe/Te.

Material	J_1	J_2	J_3	K
	(meV)			
FeSe (0 GPa)	123.1±6.5	73.0±3.3	18.3±1.8	30.6±0.4
FeSe (4 GPa)	86.9±2.4	51.9±1.2	9.7±0.6	15.7±0.2
FeSe (9 GPa)	51.1±0.7	35.4±0.3	4.9±0.2	10.4±0.1
FeTe	50.7±3.6	42.8±1.8	24.4±1.0	19.7±0.2

The parameters for FeSe are reported at three different pressures, 0 GPa, 4 GPa and 9 GPa. FeTe is reported at 0 GPa. The reported standard errors indicate the inaccuracy of the fit to the J_1–J_2–J_3–K model. Note that the exchange constants reported here are formally defined as Jm^2, and therefore include the magnetic moment amplitude.

First we analyse the J_1–J_2–J_3–K model parameters given in Table 1 and plotted in Fig. 2. The crosses in Figs 2d,e and f, show the placement of FeSe at 9 GPa, FeSe at 0 GPa and FeTe at 0 GPa, respectively, in the J_1–J_2–J_3–K phase diagram. Interestingly, for both FeSe and FeTe the calculated ground state at ambient pressure is near a phase boundary: between the staggered-dimer

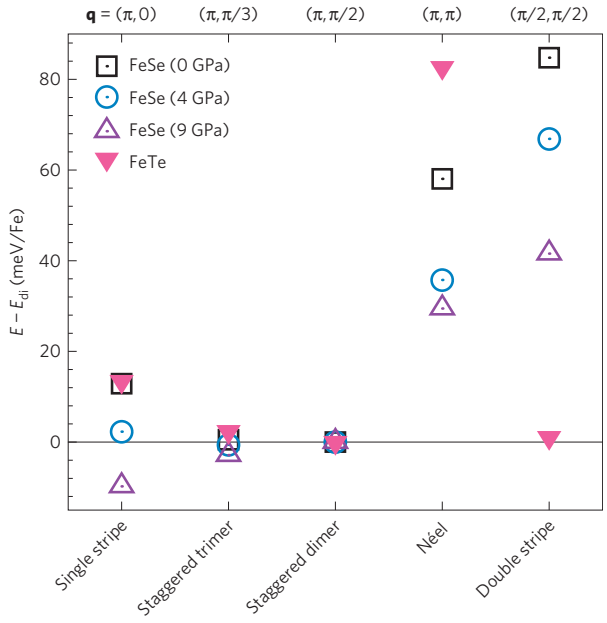

Figure 3 | Energies of collinear magnetic configurations. The total calculated DFT energies of the collinear magnetic configurations used in the fits of the J_1–J_2–J_3–K model.

phase and the single-stripe phase for FeSe (the collinear $\mathbf{q}=(\pi,Q)$, $0<Q<\pi/2$ states are all degenerate at this boundary) and between the staggered-dimer phase and double-stripe phase for FeTe. The latter seems to be very close to an Ising model because of the large K and not because of a large magnetic anisotropy.

Generally speaking, one can anticipate that, in the absence of long-range order, spin fluctuations with wavevectors corresponding to the lowest energy states will occur: thus, in FeTe one expects fluctuations with $\mathbf{q}=(\pi/2,\pi/2)$, $(\pi,\pi/2)$ and $(\pi,\pi/3)$. None of those would support $s_{\pm}$ superconductivity, as only fluctuations with $\mathbf{q}\sim(\pi,0)$ can pair electrons in the standard $s_{\pm}$ superconducting state. They all break tetragonal symmetry, but in different ways, as described below, and cannot all support the same nematic state. In FeSe, by contrast, one expects fluctuations with $\mathbf{q}=(\pi,Q)$, where $Q=0$, $\pi/4$, $\pi/3$ and $\pi/2$ (although we cannot check this, it is likely that all fluctuations with $\mathbf{q}=(\pi,Q)$, where $-\pi/2\lesssim Q\lesssim\pi/2$ are supported; see Fig. 4a). This is very different from most Fe pnictides, where the single-stripe state is much lower in energy than all other patterns, and therefore the $\mathbf{q}_{ss}$ fluctuations dominate (see the inset of Fig. 4a). We note that NaFeAs seems to be an exception and also has a near-degeneracy of these phases. The closeness of the degeneracy is, however, an artefact of using the experimental tetragonal structure of NaFeAs for the calculations. Indeed, accounting for relaxation of the lattice parameters and pnictogen heights stabilizes the single-stripe phase as the ground state (see Supplementary Methods). Interestingly, in NaFeAs both the structural/nematic and magnetic transitions occur, but the splitting is anomalous, as the nematic transition occurs at a temperature T_{nem} 40% higher than the magnetic transition T_{mag} (refs 36,37), unlike other undoped pnictides (this magnitude is similar to experimental FeSe at $P=2$ GPa). We can therefore establish a correlation between the presence of quasi-degenerate $\mathbf{q}=(\pi,Q)$ phases and the magnitude of the relative splitting between the nematic and magnetic transition temperatures $((T_{nem}-T_{mag})/T_{nem})$. Note that the above results rely on the experimental fact that Fe in FeBS has a large local moment (very close to the DFT results)[38], and cannot be obtained by linear response calculations based on a paramagnetic phase[39].

An important consequence of our findings is that the different spin fluctuations in FeSe (but not FeTe) all break the $x\leftrightarrow y$ symmetry in the same way and do not compete in terms of nematicity (this holds for all $\mathbf{q}=(\pi,Q)$, $-\pi/2\lesssim Q\lesssim\pi/2$), leading to an enhancement of the long-range nematic order. At the same time, the competing $\mathbf{q}=(\pi,Q)$ wavevectors are not compatible to magnetic ordering, and therefore naturally lead to the macroscopic suppression of long-range magnetic order observed in FeSe. This is in contrast to the case of FeTe, which orders in a double-stripe-like pattern. The double-stripe fluctuations with $\mathbf{q}_{ds}=(\pi/2,\pi/2)$ break a different symmetry, $x+y\leftrightarrow x-y$, than the $(\pi,\pi/2)$ and $(\pi,\pi/3)$ patterns, and thus they compete nematically, so there is no nematic phase present in FeTe. In conclusion, FeSe represents a rare case where several types of spin fluctuations are simultaneously excited, which prevents them from condensing at any one wavevector, but does not prevent the formation of the nematic orthorhombic order. Alternative models, relying on an itinerant scenario[40] or the role of quantum spin fluctuations[41], have also been recently suggested.

We can demonstrate quantitatively how this physics develops by using a phenomenological model that accounts for the described frustration. The key input from the DFT calculations is the fact that magnetic fluctuations with momenta transverse to the stripe ordering vector, $\mathbf{q}_{ss}=(\pi,0)$, are significantly softer than those with longitudinal momenta (see Fig. 4a). We thus model the low-energy magnetic excitations by the susceptibility $\chi^{-1}(\mathbf{q}_{ss}+\mathbf{q})=\chi^{-1}(\mathbf{q}_{ss})+q_x^2+\lambda q_y^2$, where $\chi(\mathbf{q}_{ss})\propto 1/(T-T_{mag,0})$ diverges at the mean-field magnetic transition temperature $T_{mag,0}$. λ is the parameter characterizing this magnetic softness, which is significantly smaller in FeSe than in most Fe pnictides (see inset of Fig. 4a). Indeed, recent neutron experiments on FeSe (ref. 42) reveal $\chi(\mathbf{q})$ of the above form, with $\lambda\approx 0.05$ for FeSe and $\lambda\approx 0.5$ for Co-doped $BaFe_2As_2$ (ref. 43). By going beyond mean field and consistently accounting for magnetic fluctuations (see Methods), we find that whereas the bare (that is, in the absence of nematic order) magnetic transition temperature is suppressed by the magnetic softness according to $T_{mag}-T_{mag,0}\propto-\lambda^{-(3-d)/2}$, the nematic transition is enhanced $T_{nem}-T_{mag}\propto\lambda^{-1/(4-d)}$ (d is the system's dimensionality). Therefore, as anticipated, the unique magnetic softness of FeSe suppresses long-range magnetic order at the same time as it boosts long-range nematic order.

This nematic order, just as the underlying incipient magnetic order, is accompanied by considerable orbital ordering. We find (see Fig. 4c) that all investigated $\mathbf{q}=(\pi,Q)$ states induce population imbalance between the Fe(d_{xz}) and Fe(d_{yz}) orbitals on each Fe site of the order of $(n_{xz}-n_{yz})/(n_{xz}+n_{yz})\approx 8\%$. As these states correspond to rather different wavevectors, and thus a different folding of the magnetic Brillouin zone, but trigger basically the same orbital ordering, we conclude that the latter is not sensitive to the magnetic long-range order, but only to the nematic order. The orbital ordering can be probed experimentally, and was observed in the nematic phase at $T\lesssim T_s$ by the Knight shift anisotropy[29], whereas a divergence in $1/TT_1$, as expected, was observed only at much lower temperatures, on approaching the long-range magnetic order at $T\sim 0$.

We have also calculated the density of states at the Fermi level $N(0)$ (Fig. 4b), and found it to be rather similar in all nematic-compatible states, and strongly decreased compared to the paramagnetic or Néel states. We thus observe that the immediate cause of the reduction of $N(0)$ is the orbital ordering (which is about the same in all nematic-compatible states), which itself has a magnetic origin. One can naturally conjecture that the superposition of spin fluctuations with $\mathbf{q}=(\pi,Q)$, when averaged over all Qs, has an effect similar to zone folding with $\mathbf{q}=(\pi,0)$, and, like in the stripe magnetic structure, leads to a sharp reduction in the Fermi surface and thereby $N(0)$, which is consistent with photoemission and quantum oscillation experiments[44,45].

Let us now address the effect of pressure. In general, pressure reduces magnetic interactions in FeSe. However, the staggered-dimer state is suppressed with pressure faster than the single-stripe state

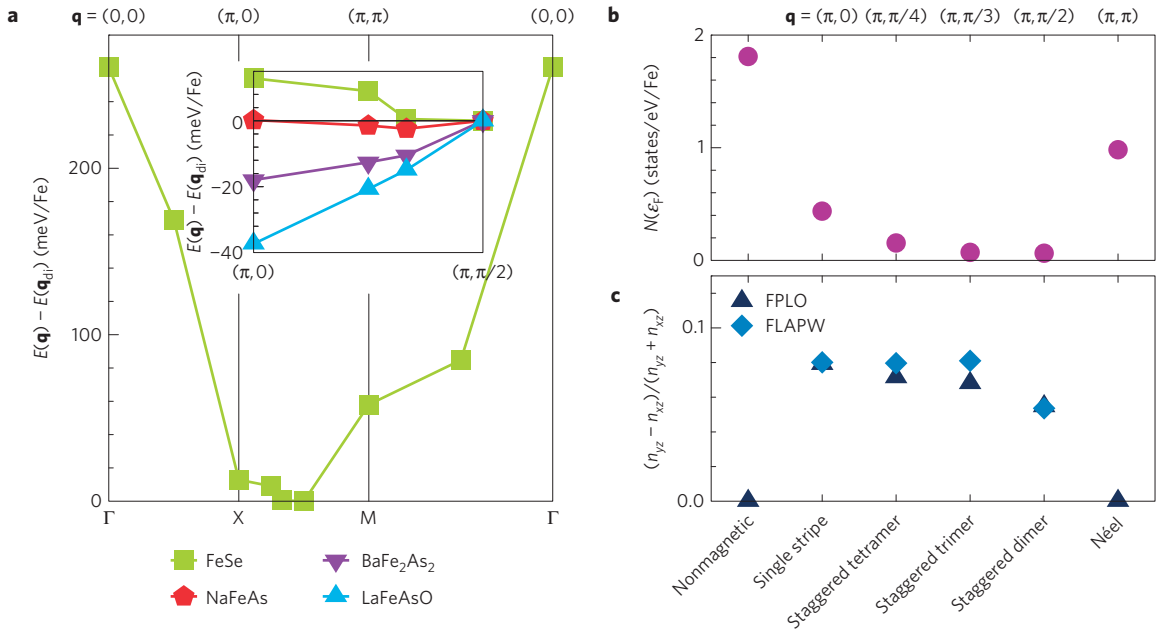

Figure 4 | Energies, density of states at ε_F and orbital order of FeSe at 0 GPa pressure. a, The energies of collinear magnetic configurations of FeSe at ambient pressure plotted as a function of **q**. Inset: The energies of FeSe, NaFeAs, $BaFe_2As_2$ and LaFeAsO (see legend) along the $\mathbf{q}=(\pi,Q)$ line, where $0\leq Q\leq\pi/2$. **b**, $N(\varepsilon_F)$ for the lowest energy magnetic configurations compared to the nonmagnetic states indicates very small Fermi surfaces in fluctuating magnetic states. **c**, Ferro-orbital order in Fe $3d_{xz}/d_{yz}$ orbitals measured for several magnetic states.

(Fig. 3), so that instead of multiple competing types of fluctuation we obtain a situation similar to the pnictides, where fluctuations with $\mathbf{q}=(\pi,0)$ dominate. Recent resistivity measurements on FeSe under pressure[46,47] identified an antiferromagnetic phase at a pressure $\gtrsim$1–2 GPa. Our calculations predict such a phase for pressures above 4 GPa, therefore showing the right behaviour, albeit with an underestimation of the critical pressure.

Note that in the $s_\pm$ model the fluctuations with $\mathbf{q}=(\pi,0)$ are responsible for superconductivity. At ambient pressure, the staggered-dimer/trimer fluctuations are dominant, but cannot lead to pairing, because the very small FeSe Fermi pockets are not connected by $\mathbf{q}=(\pi,Q)$, where $Q\sim\pi/2$. As discussed in ref. 48, such low-energy fluctuations with 'wrong' momenta are pairbreaking because they act essentially as impurities (note that the situation in FeSe is qualitatively different from previous discussions in which fluctuations in different channels compete, but can in principle each lead to pairing).

Under pressure the pairbreaking staggered-dimer and -trimer spin fluctuations are seen to decrease in amplitude much more rapidly than the pairing stripe spin fluctuations at $\mathbf{q}=(\pi,0)$. This removal of pairbreaking effects is responsible for the initial increase in T_c. The further increase of pressure decreases the amplitude of both the pairbreaking $\mathbf{q}=(\pi,Q)$ and pairing $\mathbf{q}=(\pi,0)$ fluctuations, leading to the dome-like behaviour of T_c versus pressure. Even more importantly, the nematic order, which is strongest at $P=0$, gradually weakens with pressure, as the $\mathbf{q}=(\pi,Q)$ ($Q\sim\pi/2$) fluctuations are suppressed. As discussed above, the nematic ordering (originating from magnetic fluctuations and accompanied by orbital ordering) strongly reduces $N(0)$ and therefore T_c (competition between nematicity and superconductivity has been observed experimentally in $BaFe_{2-x}Co_xAs_2$ (ref. 49)), so the suppression of nematicity with pressure is another factor ensuring the initial rise of T_c.

Conclusions

We have presented a detailed analysis, based on first-principles calculations, of magnetic interactions in the FeSe/Te family. We show that in FeSe the magnetic interactions are much more frustrated than in most FeBS, including FeTe. Using a phenomenological model to account for this frustration we showed that the simultaneous excitation of spin fluctuations with the wavevectors suggested by the calculations prevents long-range magnetic ordering in FeSe, but does allow the usual spin-driven nematic order. The spin-driven nematic order is also accompanied by a ferro-orbital order, which makes the Fermi surface and density of states deviate from the nonmagnetic DFT calculations. With pressure FeSe becomes more akin to the typical Fe pnictides, where the $(\pi,0)$ fluctuations dominate, consistent with recent observations of antiferromagnetism at higher pressure[46,47]. From the point of view of superconductivity, FeSe at $P=0$ seems to be underdoped, despite the absence of a long-range antiferromagnetism, where the competition between superconductivity and another order suppresses T_c, consistent with the experimentally observed characteristic dome structure with T_c peaked at $P=9$ GPa. We also observed that at $P=0$ the leading fluctuations are non-pairing in the $s_\pm$ channel, but pairing fluctuations become the leading fluctuations with pressure, also consistent with the initial increase of T_c with pressure.

To be able to analyse the emerging situation on a model level, we mapped the low-energy energetics onto a three-neighbour Heisenberg + biquadratic exchange Hamiltonian, which we have solved analytically at $T=0$ in the mean-field approximation. It seems that the biquadratic interaction is essential to stabilize the observed double-stripe phase in FeTe; without the extra term, this phase can never be the ground state at any choice of parameters. The same is true for the staggered-dimer phase found to be the DFT ground state in FeSe. A nontrivial combination of the biquadratic and third-neighbour exchanges, in addition to the usually considered first- and second-neighbour Heisenberg interactions, ensures the anomalously large splitting of the nematic and antiferromagnetic transitions and the suppression of magnetic ordering in FeSe. We believe that this new perspective on the unusual magnetic physics of Fe chalcogenides will be crucial to an explanation of their remarkable properties, including perhaps high-temperature superconductivity in the monolayer FeSe system.

Methods

Methods and any associated references are available in the online version of the paper.

Received 20 January 2015; accepted 13 July 2015; published online 24 August 2015

References

1. Chubukov, A. Pairing mechanism in Fe-based superconductors. *Annu. Rev. Condens. Matter Phys.* **3,** 57–92 (2012).
2. Hirschfeld, P. J., Korshunov, M. M. & Mazin, I. I. Gap symmetry and structure of Fe-based superconductors. *Rep. Prog. Phys.* **74,** 124508 (2011).
3. Wang, F., Zhai, H. & Lee, D.-H. Antiferromagnetic correlation and the pairing mechanism of the cuprates and iron pnictides: A view from the functional renormalization group studies. *Europhys. Lett.* **85,** 37005 (2009).
4. Chubukov, A. V., Efremov, D. V. & Eremin, I. Magnetism, superconductivity, and pairing symmetry in iron-based superconductors. *Phys. Rev. B* **78,** 134512 (2008).
5. Stanev, V., Kang, J. & Tesanovic, Z. Spin fluctuation dynamics and multiband superconductivity in iron pnictides. *Phys. Rev. B* **78,** 184509 (2008).
6. Kuroki, K. *et al.* Unconventional pairing originating from the disconnected Fermi surfaces of superconducting $LaFeAsO_{1-x}F_x$. *Phys. Rev. Lett.* **101,** 087004 (2008).
7. Graser, S., Maier, T. A., Hirschfeld, P. J. & Scalapino, D. J. Near-degeneracy of several pairing channels in multiorbital models for the Fe pnictides. *New J. Phys.* **11,** 025016 (2009).
8. Sknepnek, R., Samolyuk, G., Lee, Y.-B. & Schmalian, J. Anisotropy of the pairing gap of FeAs-based superconductors induced by spin fluctuations. *Phys. Rev. B* **79,** 054511 (2009).
9. Guterding, D., Jeschke, H. O., Hirschfeld, P. J. & Valentí, R. Unified picture of the doping dependence of superconducting transition temperatures in alkali metal/ammonia intercalated FeSe. *Phys. Rev. B* **91,** 041112 (2015).
10. Seo, K., Bernevig, B. A. & Hu, J. Pairing symmetry in a two-orbital exchange coupling model of oxypnictides. *Phys. Rev. Lett.* **101,** 206404 (2008).
11. Lv, W., Krüger, F. & Phillips, P. Orbital ordering and unfrustrated $(\pi,0)$ magnetism from degenerate double exchange in the iron pnictides. *Phys. Rev. B* **82,** 045125 (2010).
12. Dai, P., Hu, J. & Dagotto, E. Magnetism and its microscopic origin in iron-based high-temperature superconductors. *Nature Phys.* **8,** 709–718 (2012).
13. Moon, S. J. *et al.* Dual character of magnetism in $EuFe_2As_2$: Optical spectroscopic and density-functional calculation study. *Phys. Rev. B* **81,** 205114 (2010).
14. Lee, H., Zhang, Y.-Z., Jeschke, H. O. & Valentí, R. Possible origin of the reduced ordered magnetic moment in iron pnictides: A dynamical mean-field theory study. *Phys. Rev. B* **81,** 220506 (2010).
15. Yin, Z. P., Haule, K. & Kotliar, G. Kinetic frustration and the nature of the magnetic and paramagnetic states in iron pnictides and iron chalcogenides. *Nature Mater.* **10,** 932–935 (2011).
16. Chandra, P., Coleman, P. & Larkin, A. I. Ising transition in frustrated Heisenberg models. *Phys. Rev. Lett.* **64,** 88–91 (1990).
17. Zhao, J. *et al.* Spin waves and magnetic exchange interactions in $CaFe_2As_2$. *Nature Phys.* **5,** 555–560 (2009).
18. Diallo, S. O. *et al.* Itinerant magnetic excitations in antiferromagnetic $CaFe_2As_2$. *Phys. Rev. Lett.* **102,** 187206 (2009).
19. Yaresko, A. N., Liu, G.-Q., Antonov, V. N. & Andersen, O. K. Interplay between magnetic properties and Fermi surface nesting in iron pnictides. *Phys. Rev. B* **79,** 144421 (2009).
20. Li, S. *et al.* First-order magnetic and structural phase transitions in $Fe_{1+y}Se_xTe_{1+x}$. *Phys. Rev. B* **79,** 054503 (2009).
21. Bao, W. *et al.* Tunable $(\delta\pi,\delta\pi)$-type antiferromagnetic order in α-Fe(Te,Se) superconductors. *Phys. Rev. Lett.* **102,** 247001 (2009).
22. Ma, F., Ji, W., Hu, J., Lu, Z.-Y. & Xiang, T. First-principles calculations of the electronic structure of tetragonal α-FeTe and α-FeSe crystals: Evidence for a bicollinear antiferromagnetic order. *Phys. Rev. Lett.* **102,** 177003 (2009).
23. Ferrer, J. Spin-liquid phase for the frustrated quantum Heisenberg antiferromagnet on a square lattice. *Phys. Rev. B* **47,** 8769–8782 (1993).
24. Sindzingre, P., Shannon, N. & Momoi, T. Phase diagram of the spin-1/2 J_1–J_2–J_3 Heisenberg model on the square lattice. *J. Phys. Conf. Ser.* **200,** 022058 (2010).
25. Wysocki, A. L., Belashchenko, K. D. & Antropov, V. P. Consistent model of magnetism in ferropnictides. *Nature Phys.* **7,** 485–489 (2011).
26. Hu, J., Xu, B., Liu, W., Hao, N.-N. & Wang, Y. Unified minimum effective model of magnetic properties of iron-based superconductors. *Phys. Rev. B* **85,** 144403 (2012).
27. Fernandes, R. M., Chubukov, A. V., Knolle, J., Eremin, I. & Schmalian, J. Preemptive nematic order, pseudogap, and orbital order in the iron pnictides. *Phys. Rev. B* **85,** 024534 (2012).
28. Xu, C., Müller, M. & Sachdev, S. Ising and spin orders in the iron-based superconductors. *Phys. Rev. B* **78,** 020501 (2008).
29. Baek, S.-H. *et al.* Orbital-driven nematicity in FeSe. *Nature Mater.* **14,** 210–214 (2015).
30. Böhmer, A. E. *et al.* Origin of the tetragonal-to-orthorhombic phase transition in FeSe: A combined thermodynamic and NMR study of nematicity. *Phys. Rev. Lett.* **114,** 027001 (2015).
31. Medvedev, S. *et al.* Electronic and magnetic phase diagram of β-$Fe_{1.01}Se$ with superconductivity at 36.7 K under pressure. *Nature Mater.* **8,** 630–633 (2009).
32. Landau, D. P. & Binder, K. Phase diagrams and critical behavior of Ising square lattices with nearest-, next-nearest-, and third-nearest-neighbor couplings. *Phys. Rev. B* **31,** 5946–5953 (1985).
33. Cao, H.-Y., Chen, S., Xiang, H. & Gong, X.-G. Antiferromagnetic ground state with pair-checkerboard order in FeSe. *Phys. Rev. B* **91,** 020504 (2015).
34. Glasbrenner, J. K., Velev, J. P. & Mazin, I. I. First-principles study of the minimal model of magnetic interactions in Fe-based superconductors. *Phys. Rev. B* **89,** 064509 (2014).
35. Luo, Q. & Dagotto, E. Magnetic phase diagram of a five-orbital Hubbard model in the real-space Hartree–Fock approximation varying the electronic density. *Phys. Rev. B* **89,** 045115 (2014).
36. Parker, D. R. *et al.* Control of the competition between a magnetic phase and a superconducting phase in cobalt-doped and nickel-doped NaFeAs using electron count. *Phys. Rev. Lett.* **104,** 057007 (2010).
37. Rosenthal, E. P. *et al.* Visualization of electron nematicity and unidirectional antiferroic fluctuations at high temperatures in NaFeAs. *Nature Phys.* **10,** 225–232 (2014).
38. Mannella, N. The magnetic moment enigma in Fe-based high temperature superconductors. *J. Phys. Condens. Matter* **26,** 473202 (2014).
39. Yin, Z. P., Haule, K. & Kotliar, G. Spin dynamics and orbital-antiphase pairing symmetry in iron-based superconductors. *Nature Phys.* **10,** 845–850 (2014).
40. Chubukov, A. V., Fernandes, R. M. & Schmalian, J. Origin of nematic order in FeSe. *Phys. Rev. B* **91,** 201105 (2015).
41. Wang, F., Kivelson, S. & Lee, D.-H. Is FeSe a nematic quantum paramagnet? *Nature Phys.* **11,** http://dx.doi.org/10.1038/nphys3456 (in the press) (2015).
42. Rahn, M. C., Ewings, R. A., Sedlmaier, S. J., Clarke, S. J. & Boothroyd, A. T. Strong $(\pi,0)$ spin fluctuations in β-FeSe observed by neutron spectroscopy. *Phys. Rev. B* **91,** 180501 (2015).
43. Tucker, G. S. *et al.* Magnetic excitations in underdoped $Ba(Fe_{1-x}Co_x)_2As_2$ with $x = 0.047$. *Phys. Rev. B* **86,** 024505 (2012).
44. Terashima, T. *et al.* Anomalous Fermi surface in FeSe seen by Shubnikov–de Haas oscillation measurements. *Phys. Rev. B* **90,** 144517 (2014).
45. Watson, M. D. *et al.* Dichotomy between the hole and electrons behavior in multiband FeSe probed by ultrahigh magnetic fields. *Phys. Rev. Lett.* **115,** 027006 (2015).
46. Terashima, T. *et al.* Pressure-induced antiferromagnetic transition and phase diagram in FeSe. *J. Phys. Soc. Jpn* **84,** 063701 (2015).
47. Bendele, M. *et al.* Pressure induced static magnetic order in superconducting $FeSe_{1-x}$. *Phys. Rev. Lett.* **104,** 087003 (2010).
48. Millis, A. J., Sachdev, S. & Varma, C. M. Inelastic scattering and pair breaking in anisotropic and isotropic superconductors. *Phys. Rev. B* **37,** 4975–4986 (1988).
49. Nandi, S. *et al.* Anomalous suppression of the orthorhombic lattice distortion in superconducting $Ba(Fe_{1-x}Co_x)_2As_2$ single crystals. *Phys. Rev. Lett.* **104,** 057006 (2010).

Acknowledgements

We thank M. Tomić for running some test calculations at the initial stages of this work and D. Guterding, S. Backes, A. Coldea, A. Chubukov, N. Perkins, S. Kivelson and W. Ku for valuable discussions. I.I.M. is supported by ONR through the NRL Basic Research Program. J.K.G. acknowledges the support of the NRC Program at NRL. H.O.J. and R.V. are supported by DFG-SPP1458. P.J.H. was partially supported by US DOE DE-FG02-05ER46236. R.M.F. is supported by the US Department of Energy, Office of Science, Basic Energy Sciences, under award number DE-SC0012336. I.I.M., R.V. and P.J.H. were supported in part by KITP under NSF grant PHY11-25915.

Author contributions

I.I.M. and J.K.G. conceived the research; J.K.G., I.I.M. and H.O.J. carried out numerical calculations; R.M.F. carried out analytical calculations for the phenomenological model; all authors participated in the discussion and contributed to writing the paper; I.I.M. and R.V. supervised the whole project.

Additional information

Supplementary information is available in the online version of the paper. Reprints and permissions information is available online at www.nature.com/reprints. Correspondence and requests for materials should be addressed to J.K.G.

Competing financial interests

The authors declare no competing financial interests.

Methods

DFT calculations and fitting procedure. We employed density functional theory and made use of three separate, full potential (all electron) codes, ELK (ref. 50), WIEN2K (ref. 51) and FPLO (ref. 52) to calculate the energies. The generalized gradient approximation was used for the exchange–correlation functional[53]. We checked for convergence with respect to k-points and, for ELK, the number of empty states. We calculated the energies of multiple collinear configurations using all three codes for comparison purposes, whereas noncollinear calculations were handled exclusively by the ELK code.

We used the tetragonal $P4/nmm$ space group (origin choice 2) for the crystal structure of FeSe and FeTe in all our calculations. The Fe and chalcogenide (Se/Te) ions occupy the 2a and 2c Wyckoff positions, respectively. The lattice parameters for the different materials (and for FeSe, under different pressures, which were taken from ref. 54) are summarized in Supplementary Table I. We note that at low temperatures FeSe is strictly an orthorhombic structure, but this distortion is small, and omitting it leads to a small magnetoelastic error when compared with the exchange parameter energy scales. Furthermore, we are interested in the physics that emerges from spin fluctuations that originate in the tetragonal phase. Therefore, for FeSe, we defined a volume-conserving effective parameter $a^*=\sqrt{ab}$, where a and b are the orthorhombic parameters taken from experiment.

The structures in Supplementary Fig. 1 summarize all of the different configurations that we considered. For structures that do not have a commonly used label, such as Supplementary Fig. 1h, we named them using a generic scheme, where black circles are up (u) and ×s are down (d). To construct the generic name, we start with the bottom row, read the pattern from left to right, then move up a row and repeat (hyphens are used to distinguish between rows in the pattern).

Supplementary Fig. 2 gives the energies we calculated using these codes. Note that we did not calculate the energy of every configuration using all three codes, but there are several points of comparison. For all configurations for which we can make a comparison, there is excellent agreement across codes. Across the different codes there is no ambiguity as to the energy hierarchy of the low-lying energy states. In addition, the energy range for the different configurations is fairly large for both FeSe and FeTe, on the scale of 100–300 meV for FeSe and 50–100 meV for FeTe.

We fit to the Hamiltonian in equation (1) using the ordinary least squares method. The coefficients for the collinear Heisenberg model obtained by summing over neighbours are reported in Supplementary Table II. For the noncollinear calculations used to obtain the biquadratic parameter K, the model reduces to $\Delta E(\theta)=E(\theta)-E(0)=2K\sin^2(\theta)$; see ref. 34 for the definition of θ. The noncollinear energies and the corresponding fits are shown in Supplementary Fig. 3.

It was not possible to achieve a fit that accurately reproduced all energies for all possible collinear configurations. This is a consequence of the itinerant nature of the magnetism, which in general cannot be mapped onto a pairwise interaction model. We also note that the lower symmetry magnetic structures, such as those with generic names like 'uudd-dudd-dduu-dddu,' suffered moment collapse in FeSe under pressure. To control these difficulties, we defined a set of four criteria for our fitting procedure. The criteria were collinear ground states of the J_1–J_2–J_3–K model should be included; low-energy structures that do not suffer from moment collapse under pressure (for FeSe) should be included; local moments of included structures should be similar; and we exclude configurations that yield fits that do not reproduce the density functional theory energy hierarchy of the lowest energy configurations. The last criterion is necessary because we cannot produce an accurate fit for all configurations, so we decide which features of the density functional theory set of energies are important from the point of view of fluctuations and frustration, which are the lowest energy ones. Given these criteria, we perform the fitting procedure using the energies summarized in Fig. 3.

Finally, it is worth noting that for itinerant magnets the exchange model could be potentially improved using an approach similar to Moriya[55], and allowing the moment amplitudes to vary, and by also including Stoner-like on-site terms. We tried including terms such as this to see how it affected the quality of our fits. We found that including these terms does not change the fitting results in any qualitative way when using the configurations in Fig. 3. Furthermore, it did not allow us to extend the fit to also reproduce the high-energy configurations from Supplementary Fig. 1. It is possible, however, that these modifications would be important for fluctuations above the Néel temperature.

Phenomenological model for the nematic and magnetic transitions. Here we give the details of the phenomenological model used to calculate the magnetic and nematic transition temperatures $T_{\rm mag}$ and $T_{\rm nem}$. We start with the low-energy Ginzburg–Landau action for the magnetic degrees of freedom[27]:

$$S_{\rm eff}[M_i]=\int_q\sum_i\chi_{i,q}^{-1}\mathbf{M}_{i,q}\cdot\mathbf{M}_{i,-q}+\frac{u}{2}\int_x(M_1^2+M_2^2)^2-\frac{g}{2}\int_x(M_1^2-M_2^2)^2$$

Here, $\mathbf{M}_i$ are the magnetic order parameters corresponding to the stripe ordering vectors $\mathbf{Q}_1=(\pi,0)$ and $\mathbf{Q}_2=(0,\pi)$ (see Supplementary Discussion for the reasoning for the use of these particular momenta), $u>0$, $g>0$ are Ginzburg–Landau coefficients, and $\int_q=T\sum_n\int{\rm d}^dq/(2\pi)^d$, $\int_x=\int_0^\beta{\rm d}\tau\int{\rm d}^dx$. As explained in the main text, the susceptibilities are given by $\chi^{-1}_{1,\mathbf{Q}_1+\mathbf{q}}=r_0+q_x^2+\lambda q_y^2$ and $\chi^{-1}_{2,\mathbf{Q}_2+\mathbf{q}}=r_0+\lambda q_x^2+q_y^2$, with $r_0=a(T-T_{\rm mag,0})$, where $a>0$ and $T_{\rm mag,0}$ is the mean-field magnetic transition temperature. This expression was derived from a microscopic toy model in ref. 27; here, we use the input from the DFT calculations to phenomenologically modify the magnetic susceptibility to include the fact that magnetic fluctuations are softer along the direction transverse to the ordering vector. Within our model, this is accomplished by the parameter $\lambda>0$. Our goal here is to focus solely on the effect of λ on the nematic and magnetic transition temperatures, to mimic the difference between FeSe ($\lambda\ll1$) and the other Fe pnictides ($\lambda\sim1$). We here ignore quantum fluctuations and focus on the classical behaviour.

To obtain separate magnetic and nematic transitions, we need to go beyond mean field and take into account the effects of fluctuations. We do that self-consistently by introducing two Hubbard–Stratonovich fields ψ and φ, whose mean values are proportional to the Gaussian fluctuations, $\langle\psi\rangle\propto\langle M_1^2+M_2^2\rangle$, and to the nematic order parameter, $\langle\varphi\rangle\propto\langle M_1^2-M_2^2\rangle$. Within the saddle-point approximation, we obtain the self-consistent equations[27]:

$$\psi=\frac{u}{2}\int_q\left(\tilde{\chi}_{1,q}+\tilde{\chi}_{2,q}\right)$$

$$\varphi=\frac{g}{2}\int_q\left(\tilde{\chi}_{1,q}-\tilde{\chi}_{2,q}\right)\qquad(2)$$

where $\tilde{\chi}_{i,q}^{-1}=\chi_{i,q}^{-1}+\psi\mp\varphi$ are the renormalized magnetic susceptibilities. We first study the suppression of the mean-field magnetic transition temperature in the absence of nematic order. Setting $\varphi=0$, we find that the renormalized magnetic transition takes place when $r_{0,\rm mag}\equiv a(T_{\rm mag}-T_{\rm mag,0})=-\psi$:

$$r_{0,\rm mag}=-\bar{u}\int_0^\Lambda\int_0^\Lambda\frac{q_1^{d-2}{\rm d}q_1{\rm d}q_2}{q_1^2+\lambda q_2^2}\qquad(3)$$

Here, $(\bar{u}/u)=(2S_{d-1}T_{\rm mag,0}/(2\pi)^d)$, where Λ is the upper momentum cutoff of the theory and S_{d-1} is the area of the unit hypersphere in $(d-1)$ dimensions. Because magnetic transitions cannot happen in $d=2$, we extended the model to an arbitrary dimensionality $2<d\leq3$. The case $d=3$ corresponds to a completely isotropic system; for an anisotropic layered system, such as the FeBS, one can effectively consider a fractional dimension $2<d<3$, as shown for instance in ref. 27, to mimic the effect of the inter-layer coupling.

Let us first consider the extreme case of $\lambda=0$. As shown in equation (3), in this case the system effectively 'loses' one dimension and the lower critical dimension, where Mermin–Wagner theorem applies, increases from $d=2$ to $d=3$. This simple observation shows the strong effect that $\lambda\ll1$ has on the magnetic transition. For a finite λ, a straightforward calculation gives:

$$T_{\rm mag}-T_{\rm mag,0}=-\left(\frac{\bar{u}\Lambda^{d-2}}{a}\right)\lambda^{-(3-d)/2}f(\lambda)$$

with the 'scaling function' ($2<d<3$):

$$f(\lambda)=\frac{\lambda^{-d/2}}{2(d-2)}\left[-\frac{\pi\lambda^{d/2}}{\cos\left(\frac{\pi d}{2}\right)}+2\lambda\arctan\sqrt{\lambda}\right.$$

$$\left.-\frac{2\lambda^{3/2}}{3-d}F_{21}\left(1,\frac{3-d}{2},\frac{5-d}{2},-\lambda\right)\right]$$

where F_{21} is the hypergeometric function. For $d=3$, we obtain:

$$f(\lambda)=\frac{\arctan\sqrt{\lambda}}{\sqrt{\lambda}}+\frac{1}{2}\log\left(1+\frac{1}{\lambda}\right)$$

Therefore, $f(\lambda\to0)$ remains finite and non-zero for $2<d<3$, implying that $T_{\rm mag}-T_{\rm mag,0}\propto-\lambda^{-(3-d)/2}$. As a result, the magnetic transition temperature (in the absence of nematic order) is strongly suppressed by $\lambda\ll1$. Note that, in the extreme case $d=3$, $f(\lambda\to0)$ is singular and $T_{\rm mag}-T_{\rm mag,0}\propto-\log(1/\lambda)$. This shows that, indeed, $d=3$ is the lower critical dimension of the problem with $\lambda=0$.

We can also study the effect of λ on the nematic transition temperature. Because this is an Ising-like degree of freedom, it is not subject to the effects discussed above and related to the Mermin–Wagner theorem (for $2<d<3$). In this case, the dependence on λ is parametrical, and non-singular in this regime. Therefore, here we consider the case $\lambda>0$ (that is, moderate softness) and $2<d<3$. Defining $r=r_0+\psi$ and $\tilde{r}_0=r_0-r_{0,\rm mag}\equiv a(T-T_{\rm mag})$, we obtain from equation (2):

$$r=\tilde{r}_{0,\rm nem}-\frac{\tilde{u}}{\sqrt{\lambda}}\left[(r+\varphi)^{\frac{d-2}{2}}+(r-\varphi)^{\frac{d-2}{2}}\right]$$

$$\varphi=\frac{\tilde{g}}{\sqrt{\lambda}}\left[(r+\varphi)^{\frac{d-2}{2}}-(r-\varphi)^{\frac{d-2}{2}}\right]$$

where

$$\frac{\tilde{u}}{u}=\frac{\tilde{g}}{g}=\frac{T_{\mathrm{mag},0}S_d\pi}{4(2\pi)^d\sin\left(\frac{(d-2)\pi}{2}\right)}$$

Linearizing in φ and solving for $\tilde{r}_{0,\mathrm{nem}}\equiv a(T_{\mathrm{nem}}-T_{\mathrm{mag}})$ gives:

$$T_{\mathrm{nem}}-T_{\mathrm{mag}}=\frac{1}{a}\left[1+\frac{2u}{(d-2)g}\right]\left[\frac{(d-2)\tilde{g}}{\sqrt{\lambda}}\right]^{\frac{2}{4-d}}$$

Therefore, we obtain an enhancement of the nematic transition temperature, $T_{\mathrm{nem}}\propto\lambda^{-1/(4-d)}$. Note that the limit $\lambda\to 0$ cannot be properly attained by this expression. In fact, $\lambda=0$ effectively reduces the dimensionality of the system by one, which for $2<d<3$ should still give a finite-temperature Ising transition. Yet, the expression above clearly shows that smaller values of λ do not suppress T_{nem}. Instead, T_{nem} is enhanced by the softness of the magnetic fluctuations. Finally, note that T_{mag} refers to the magnetic transition temperature in the absence of nematic order. Once nematic order sets in, it tends to renormalize the magnetic transition temperature to higher values[27].

References

50. Dewhurst, K. *et al.* ELK FP-LAPW Code http://elk.sourceforge.net (Halle and Uppsala, 2009).
51. Blaha, P., Schwarz, K., Madsen, G. K. H., Kvasnicka, D. & Luitz, J. *WIEN2k, an Augmented Plane Wave + Local Orbitals Program for Calculating Crystal Properties* (Techn. Univ. Wien, 2001).
52. Koepernik, K. & Eschrig, H. Full-potential nonorthogonal local-orbital minimum-basis band-structure scheme. *Phys. Rev. B* **59,** 1743–1757 (1999).
53. Perdew, J. P., Burke, K. & Ernzerhof, M. Generalized gradient approximation made simple. *Phys. Rev. Lett.* **77,** 3865–3868 (1996).
54. Margadonna, S. *et al.* Pressure evolution of the low-temperature crystal structure and bonding of the superconductor FeSe ($T_c=37$ K). *Phys. Rev. B* **80,** 064506 (2009).
55. Moriya, T. *Spin Fluctuations in Itinerant Electron Magnetism* (Springer, 1985).

nature physics

SUPPLEMENTARY INFORMATION

DOI: 10.1038/NPHYS3434

Effect of magnetic frustration on nematicity and superconductivity in iron chalcogenides

J. K. Glasbrenner,[1*] I. I. Mazin,[2] Harald O. Jeschke,[3] P. J. Hirschfeld,[4] R. M. Fernandes[5], and Roser Valentí[3]

[1] *National Research Council/Code 6393, Naval Research Laboratory, Washington, DC 20375, USA*

[2] *Code 6393, Naval Research Laboratory, Washington, DC 20375, USA*

[3] *Institut für Theoretische Physik, Goethe-Universität Frankfurt, 60438 Frankfurt am Main, Germany*

[4] *University of Florida, Gainsville, FL, USA*

[5] *School of Physics and Astronomy, University of Minnesota, Minneapolis, MN 55455, USA and*

[*] *e-mail: james.glasbrenner.ctr@nrl.navy.mil*

(Dated: June 30, 2015)

Effect of lattice relaxation and pnictide/chalcogenide heights on energy hierarchy of $\mathbf{q} = (\pi, Q)$ phases

In the main text, we presented the energies of the $\mathbf{q} = (\pi, 0)$, $(\pi, \pi/2)$, $(\pi, \pi/3)$, and $(\pi, \pi/4)$ states for different pnictides as well as FeSe in the inset of Fig. 4**a**. These calculations were performed using the tetragonal experimental lattice parameters and As/Se heights for the considered materials (LaFeAsO, $BaFe_2As_2$, NaFeAs, and FeSe), and we found that NaFeAs, with these parameters, is nearly degenerate for $\mathbf{q} = (\pi, Q)$, where $0 < Q < \pi/2$, which would suggest that NaFeAs should also have no magnetic ordering similar to FeSe. Yet, in experiment the ground state is the $\mathbf{q} = (\pi, 0)$ phase. We saw that, in the case of FeTe, allowing for lattice relaxations drove the system away from the staggered dimers phase into the double stripe phase, so a similar mechanism could be at play here.

We checked this by performing a volume-conserving full optimization of NaFeAs for single stripe, staggered dimers, and staggered trimers, allowing the lattice vectors and ionic heights to relax. In all instances the obtained orthorhombic distortion was $\sim 0.5\%$, which is an order of magnitude larger than experiment, where it is $\sim 0.03\%$. The degree of orthorhombicity also varied from pattern to pattern, obtaining 0.44% for single stripe, 0.52% for staggered dimers, and 0.63% for staggered trimers. There was variation in the c parameter as well, with 6.94 Å, 7.05 Å, and 7.03 Å for single stripe, dimers, and trimers, respectively. The energies of the patterns were 0, 5.3 meV/Fe, and 1.9 meV/Fe for single stripe, dimers, and trimers, respectively, with single stripe taken as the zero. So we see that allowing for relaxation stabilizes the single stripes. In principle, since we are deep in the nematic state, magnetoelastic coupling should be taken into account, and this contributes to the stabilization of the single stripe in NaFeAs. However, just as in the main text, our results here are qualitative, as the orthorhombic distortion is much larger than seen in experiment.

In our NaFeAs calculations, the variation in the c parameter and, by extension, the ionic heights affected the energy hierarchy of the $\mathbf{q} = (\pi, Q)$ states. Manually increasing the c parameter for NaFeAs raised the energy of the single stripe phase relative to the dimers phase. On the other hand, having an orthorhombic cell versus a tetragonal cell had little effect, assuming that volume is conserved. We found that, if we took our orthorhombic cells and made them tetragonal (in the same way as was done with FeSe at 4 and 9 GPa in the main text), the energy changed by only $\sim 0.1 - 0.2$ meV/Fe.

In general we also found that the degeneracy of the $\mathbf{q} = (\pi, Q)$ phases correlates with the pnictide/chalcogenide height. In Suppl. Table IV, we summarized the distance between Fe and As planes for a representative material in the 111, 1111, and 122 structures, and the distance between Fe and Se planes in FeSe and FeTe. Comparing the heights with the energies in the inset of Fig. 4**a** in the main text, we see that for small heights, such as LaFeAsO and $BaFe_2As_2$, that the single stripe is much lower in energy than other values of Q. On the opposite end we have FeTe with a very large height, in which case the double stripe phase is lowest in energy. The heights for FeSe and NaFeAs are an intermediate range, and for these materials the near-degeneracy occurs.

Phase boundaries of J_1-J_2-J_3-K model

In the main text we summarized the details of the J_1-J_2-J_3-K model. Here we give additional details of the analytic solution. First, let us ignore the K term and refresh what is known about the $J_1 - J_2 - J_3$ Ising and Heisenberg models. The Ising model has four phases, the Néel checkerboard (cb) phase in Suppl. Fig. 1**a**, the double stripe (ds) phase in Suppl. Fig. 1**d**, the single stripe (ss) phase in Suppl. Fig. 1**e**, and the staggered dimers (di) phase in Suppl. Fig. 1**f**. The Heisenberg model also has four phases, but neither the ds or di phase are ground states in the phase diagram. Instead, the four phases are the aforementioned cb and ss phases, and in addition two spiral phases with spins rotating away from the origin as $\alpha = n_x q_x + n_y q_y$, the first with wavevector $\mathbf{q}_1 = (\pi, Q)$ and the second with $\mathbf{q}_2 = (Q, Q)$ (see, e.g., Ref.[1]). Note that at $\mathbf{q}_1(Q \to 0) = (\pi, 0)$, which is the ss phase, and at $\mathbf{q}_1(Q \to \pi) = \mathbf{q}_2(Q \to \pi) = (\pi, \pi)$, which is the cb phase. In both phases Q depends on the exchange parameters: $Q = \cos^{-1}\left[\left(2J_2 - J_1\right)/4J_3\right]$ for $\mathbf{q}_1$ and $Q = \pi - \cos^{-1}\left[J_1/\left(2J_2 + 4J_3\right)\right]$ for $\mathbf{q}_2$. Finally, the analytic expressions for the phase boundaries are summarized in Suppl. Table III.

Adding in the biquadratic term $-K\left(\hat{\mathbf{m}}_i \cdot \hat{\mathbf{m}}_j\right)^2$ restores the ds and di configurations to the phase diagram. The allowed wavevectors in the spin spiral phases also become dependent on K: $Q = \cos^{-1}\left[\left(2J_2 - J_1\right)/\left(4J_3 - 2K\right)\right]$ for $\mathbf{q}_1$ and $Q = \pi - \cos^{-1}\left[J_1/\left(2J_2 + 4J_3 - 2K\right)\right]$ for $\mathbf{q}_2$. The analytic expressions for the phase boundaries also change

DOI: 10.1038/NPHYS3434

and many become K-dependent as summarized in the last column of Suppl. Table III. As K grows so do the areas of stability of the ds and di phases. Once $K > J_1/2$, the phase diagram becomes indistinguishable from the Ising model.

$FeSe_{0.5}Te_{0.5}$

A notable omission to our results is the case of $FeSe_{0.50}Te_{0.50}$. Unlike the other materials, the structure of $FeSe_{0.50}Te_{0.50}$ is not well-defined. A common approach is to use lattice parameters from experiment and then choose the chalcogenide to be either pure Se or pure Te, assuming that the change in the lattice parameters drives the relevant physics, such as inducing superconductivity. A check of this reveals that this is not entirely the case; there is a significant energy splitting of the checkerboard, double stripe, and zig-zag configurations when Se/Te are swapped, and the energy splits are not in the same direction. Using Te lowers the checkerboard energy, while it increases the double stripe energy, for example. Furthermore, careful experimental analysis reveals that $FeSe_{0.50}Te_{0.50}$ is a disordered structure with different heights for Se and Te[2]. Taking this into account requires an expensive and non-trivial averaging procedure. While a description of $FeSe_{0.50}Te_{0.50}$ would be useful, we put the question aside for now due to the complexity of the structure.

Comment on the basis of the phenomenological model

When reviewing the construction of the phenomenological model, one may ask why the model used $\mathbf{q} = (\pi, 0)$ as the reference momentum as opposed to $\mathbf{q} = (\pi, \pm\pi/2)$, which is the DFT ground state of FeSe at ambient pressure. The reason for building the model this way is because the relevant degeneracy region ranges from $\mathbf{q} = (\pi, -Q)$ to $\mathbf{q} = (\pi, Q)$, where Q is somewhat larger than $\pi/4$ but is much smaller than π. The simplest analytic version of this is a flat-bottom curve centered at $\mathbf{q} = (\pi, 0)$. It is true that more accurate models are possible, such as a shallow double-well curve with the wells positioned near $\mathbf{q} = (\pi, \pm\pi/2)$ that would better replicate the DFT calculations. However, using such a model would add significant complexity to the theoretical treatment. Since the model itself is phenomenological and our aim was to understand qualitative effects, we decided it was best to stick with the simpler version. The important point is that only with a nearly continuous degeneracy is the magnetic transition truly suppressed.

[1] Pimpinelli, A. & Rastelli, E. Absence of long-range order in three-dimensional spherical models. *Phys. Rev. B* **42**, 984 (1990).

[2] Louca, D. *et al.* Local atomic structure of superconducting $FeSe_{1-x}Te_x$. *Phys. Rev. B* **81**, 134524 (2010).

Material	a (Å)	c (Å)	z_{Se}	z_{Te}
FeSe	3.76976	5.52122	0.2688	
FeTe	3.81362	6.25381		0.2829
FeSe (4 GPa)	3.6717	5.1943	0.2740	
FeSe (9 GPa)	3.6049	5.0304	0.2839	

TABLE I: **Crystal parameters for FeSe and FeTe.** The structure parameters and Wyckoff positions for FeSe/Te, with FeSe reported at three different pressures.

Configuration	J_1	J_2	J_3	Const.
Checkerboard	-2	2	2	1
Single Stripes	0	-2	2	1
Double Stripes	0	0	-2	1
Dimers	-1	0	0	1
Trimers	-2/3	-2/3	2/3	1

TABLE II: **The J_1, J_2, and J_3 coefficients.** The coefficients obtained by summing over neighbors of the magnetic structures used for fitting to the J_1-J_2-J_3-K model.

Phase boundary	Ising	Heisenberg	J_1-J_2-J_3-K
cb/di	$2J_3+2J_2-J_1$		$2J_3+2J_2-J_1$
cb/ss			
ss/di	$2J_3-2J_2+J_1$		$4J_3-2J_2+J_1-2K$
di/ds	$2J_3-J_1$		$2J_3-J_1$
cb/$\mathbf{q}=(\pi,Q)$		$4J_3+2J_2-J_1$	$4J_3+2J_2-J_1-2K$
ss/$\mathbf{q}=(\pi,Q)$		$4J_3-2J_2+J_1$	$4J_3-2J_2+J_1-2K$
cb/$\mathbf{q}=(Q,Q)$		$4J_3+2J_2-J_1$	$4J_3+2J_2-J_1-2K$
$\mathbf{q}=(\pi,Q)$/$\mathbf{q}=(Q,Q)$		$2J_3-J_2$	$2J_3-J_2-K$
di/$\mathbf{q}=(\pi,Q)$			$4K(2J_3-K)-(2J_2-J_1)^2$
di/$\mathbf{q}=(Q,Q)$			$(J_1-J_2-4J_3+3K)^2-J_1(J_1+J_2+K)+2J_1^2$
ds/$\mathbf{q}=(\pi,Q)$			$8J_3(2J_3-J_1)-(2J_2-J_2)^2-(2K-J_1)^2+J_1^2$
ds/$\mathbf{q}=(Q,Q)$			$8J_3K+4J_2K-4K^2-J_1^2$

TABLE III: **Analytical solutions for phase boundaries of the Ising, Heisenberg, and J_1-J_2-J_3-K models.**

Material	Fe-As/Se Distance (Å)
LaFeAsO	1.32
$BaFe_2As_2$	1.36
NaFeAs	1.43
FeSe (0 GPa)	1.48
FeSe (4 GPa)	1.42
FeSe (9 GPa)	1.42
FeTe	1.77

TABLE IV: Distance between Fe and As/Se planes for selected pnictides and chalcogenides.

DOI: 10.1038/NPHYS3434

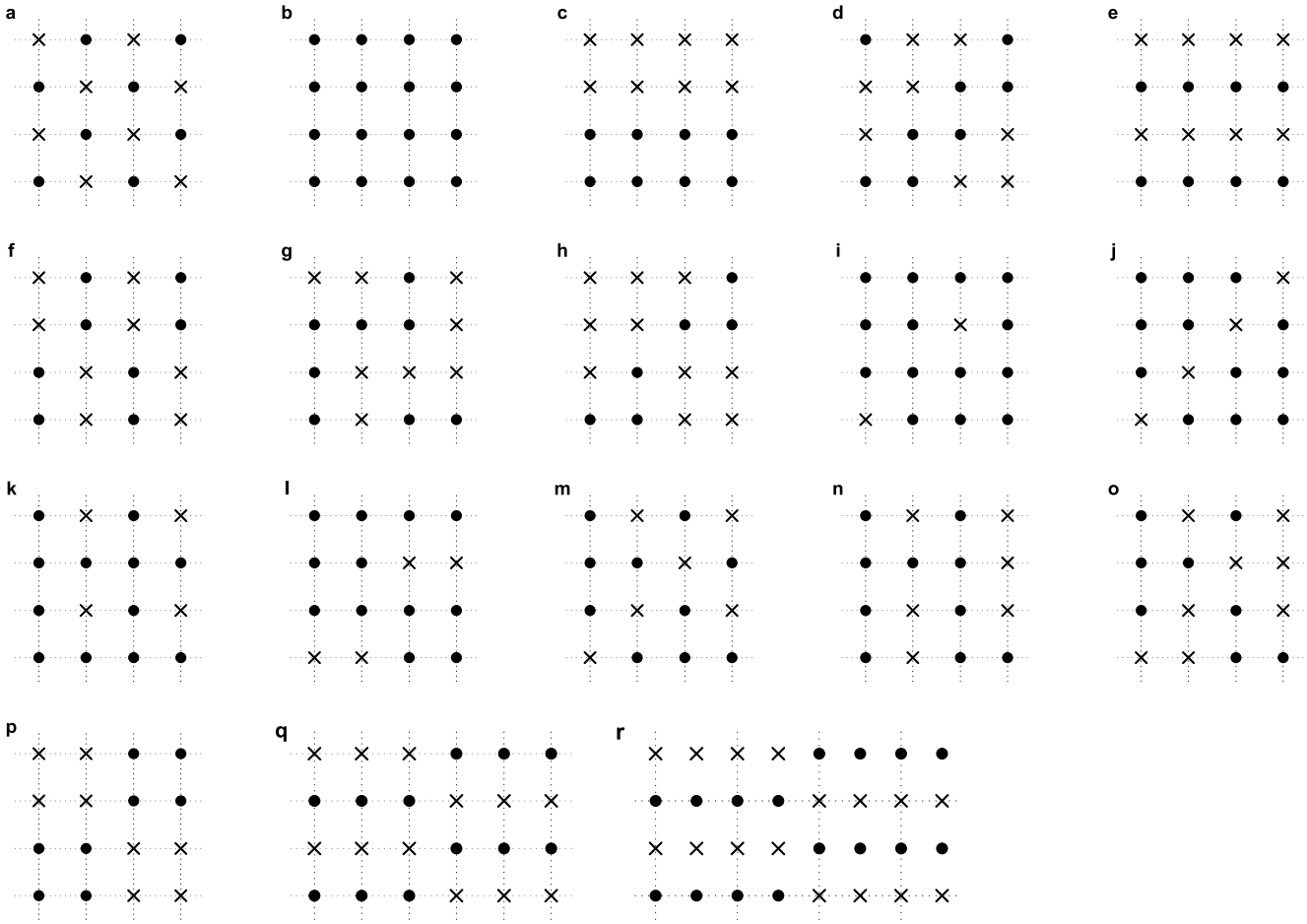

FIG. 1: **Collinear magnetic structures** **a**, Checkerboard (cb). **b**, Ferromagnetic (fm). **c**, Parallel Stripes (parastr). **d**, Double Stripe (ds). **e**, Single Stripe (ss). **f**, Staggered Dimers (di). **g**, Zig-zag Stripes (zigzag). **h**, uudd-dudd-dduu-dddu. **i**, duuu-uuuu-uudu-uuuu. **j**, duuu-uduu-uudu-uuud. **k**, uuuu-udud-uuuu-udud. **l**, dduu-uuuu-uudd-uuuu. **m**, duuu-udud-uudu-udud. **n**, uduu-udud-uuud-udud. **o**, dduu-udud-uudd-udud. **p**, plaquette (plaq). **q**, Staggered Trimers (tri). **r**, Staggered Tetramers (tet).

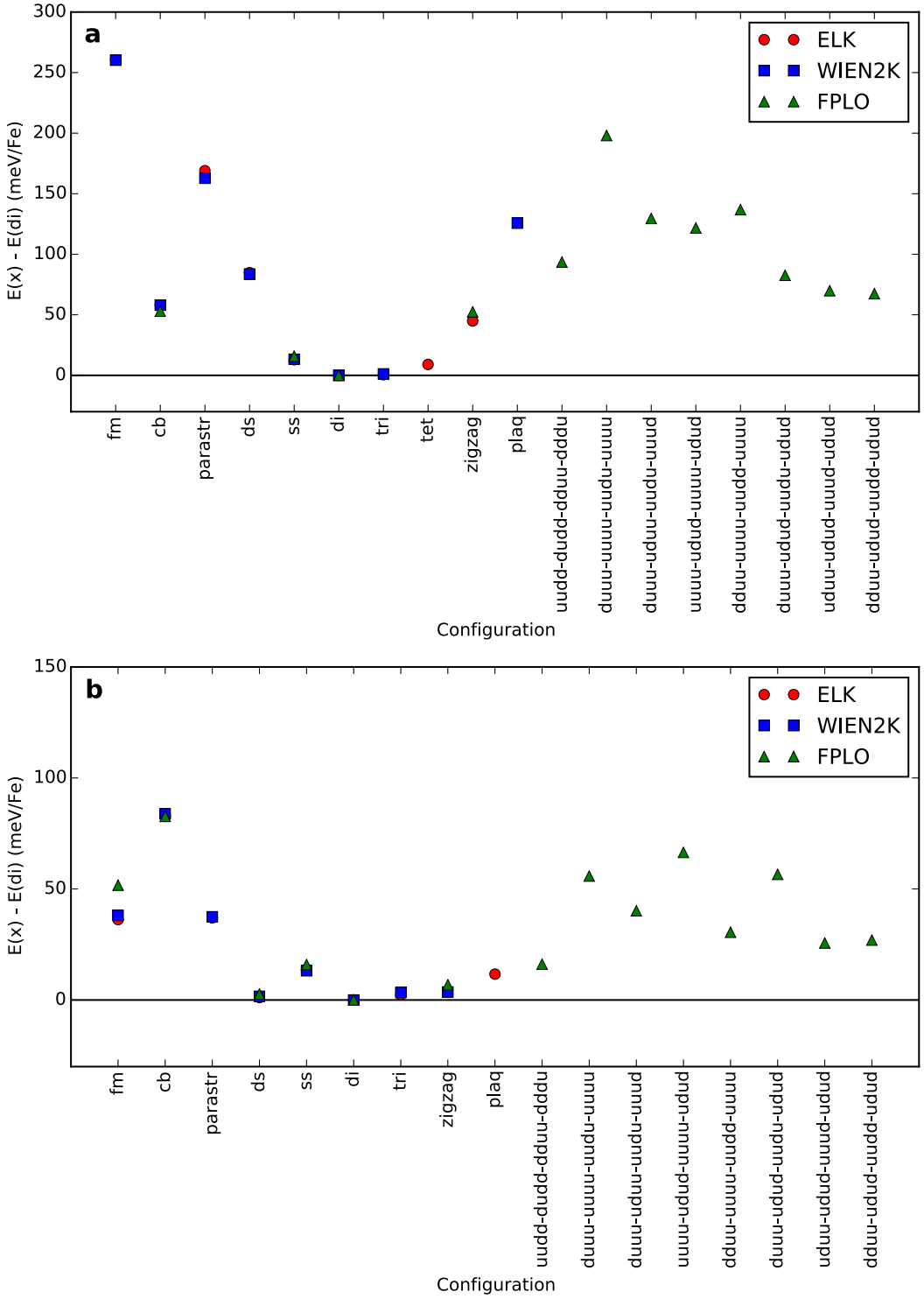

FIG. 2: **Comparison of DFT energies** The DFT energies were calculated using ELK, WIEN2K, and FPLO. **a**, FeSe. **b**, FeTe.

DOI: 10.1038/NPHYS3434

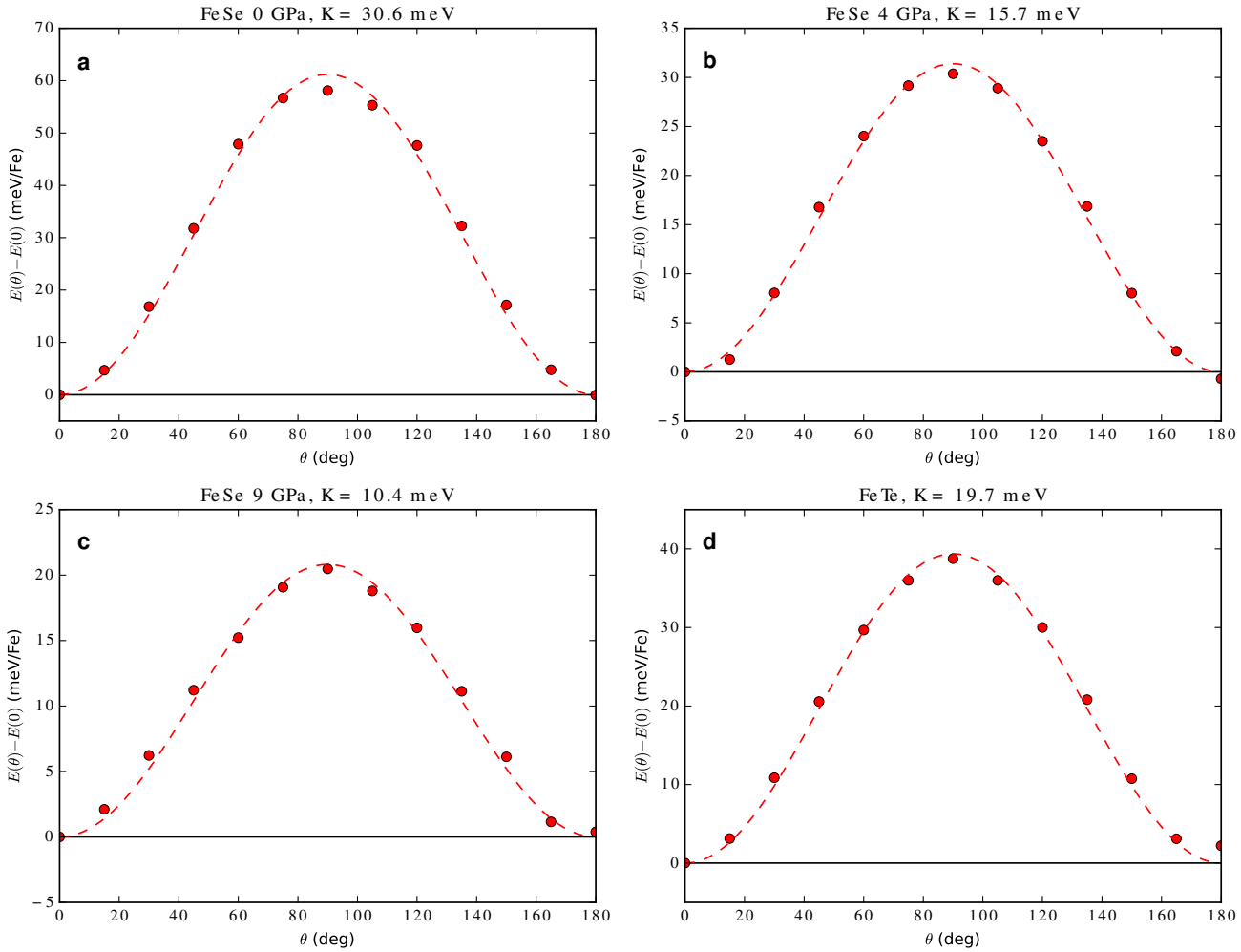

FIG. 3: **Energies of noncollinear structures for FeSe and FeTe as a function of the rotation angle.** The dashed lines are the model fits. **a**, FeSe at 0 GPa pressure. **b**, FeSe at 4 GPa pressure. **c**, FeSe at 9 GPa pressure. **d**, FeTe.